JOURNAL OF CATALYSIS **177,** 72–81 (1998)
ARTICLE NO. CA982088

Structure of Molybdenum Supported on α-, γ-, and χ-Aluminas in Relation to Its Epoxidation Activity

S. Imamura,*[,1] H. Sasaki,* M. Shono,* and H. Kanai†

*Department of Chemistry, Kyoto Institute of Technology, Matsugasaki, Sakyo-ku, Kyoto 606, Japan; and †Department of Environmental Information, Kyoto Prefectural University, Shimogamo, Sakyo-ku, Kyoto 606, Japan

Received September 23, 1997; revised January 9, 1998; accepted March 26, 1998

The structures of Mo supported on α-, γ-, and χ-aluminas were analyzed by ESCA, XRD, IR, and XAFS techniques, and the relationship between the structure of Mo and its catalytic activity for the epoxidation of allyl alcohol was discussed. The ranges of the Mo-monolayer formation as estimated by the ESCA technique were less than 18, 15, and 1 wt% of Mo-loading for γ-, χ-, and α-aluminas, respectively. However, MoO_3 was detected by an XRD analysis at 10 wt% of Mo-loading for γ- and χ-aluminas; the ESCA technique overestimated the range of the monolayer. The monolayer on γ- and χ-aluminas as apparently determined by the ESCA analysis consisted of isolated tetrahedral Mo, octahedral polymolybdate, and a small amount of MoO_3. The monolayer on α-alumina contained only tetrahedral Mo-species. MoO_3 was predominantly formed after the completion of the monolayer on all aluminas. The epoxidation activity of Mo was low in the monolayer region; especially, isolated tetrahedral Mo was completely inactive. MoO_3 was the most active species for the epoxidation, and peroxo-type oxygen bound to Mo was deduced to be the active species.

INTRODUCTION

Molybdenum (Mo) is used as catalysts in a number of reactions such as hydrogenolysis and hydrodesulfrization of crude oil (1, 2), metathesis of olefins (3), partial oxidation of olefins and alcohols (4–8), hydrogenation of benzene (9). As the state of Mo varies much depending upon the kind of supports and the methods of loading, the structures of the supported Mo have been extensively investigated by a variety of techniques such as UV spectroscopy (10), IR technique (11–13), ESR spectroscopy (14), ion scattering spectroscopy (15, 16), XPS (17–21), laser Raman spectroscopy (10, 18, 22, 23), inelastic neutron scattering analysis (24), XAFS (25–31), and NMR techniques (17, 32, 33). Alumina is the most frequently used support for Mo. Mo-monolayer is formed on alumina in the low Mo-loading region, and the monitoring of the range of this monolayer is very important in analyzing the state of Mo. Desikan *et al.* and other researchers determined the exposed Mo surface area by adsorption of oxygen, CO, and CO_2 (23, 34–40). Gil-Llambias *et al.* measured the coverage of alumina with MoO_3 by PZC (point of zero charge) method (41), and Niwa *et al.* determined the exposed alumina surface by the adsorption of benzoate compounds which interacts selectively with alumina (42). The mode of the formation of the monolayer can also be monitored by the intensity ratio of the ESCA spectra of Mo and Al (I_{Mo}/I_{Al}) (2, 17). It is generally noted that Mo species formed on the surface of alumina are isolated tetrahedral Mo, octahedral polymolybdate, and MoO_3. Mo is present in the forms of heptamolybdate ($Mo_7O_{24}^{6-}$) and monomeric MoO_4^{2-} at an equilibrium in an aqueous phase [$Mo_7O_{24}^{6-} + 4H_2O \rightleftarrows 7MoO_4^{2-} + 8H^+$] (22, 43). MoO_4^{2-} is preferentially adsorbed on the basic hydroxyl groups present on alumina and, thus, isolated tetrahedral species is formed at very low Mo-loading (10, 34). After consumption of the hydroxyl groups octahedral polymolybdate is produced (10, 12, 22, 44), and when the monolayer is completed $Al_2(MoO_4)_3$ begins to be formed, followed by subsequent formation of crystalline MoO_3 at higher Mo-loading (45). XAFS analysis gives more direct and useful information on the structures of Mo. Clausen *et al.* suggested the presence of disordered form of Mo (isolated ions, chains, or very fine patches) supported on η-alumina with 8.6 wt% loading. This EXAFS Fourier Transform shows the presence of only one Mo–O bond of about 1.7 Å length, and no significant ordered structure exists outside the first oxygen coordination shell (26). Verbruggen *et al.* investigated the effect of potassium ion on the depolymerization of polymolybdate present in the Mo-monolayer (29). The relationship between the nature of the adsorption site on alumina and the structure of Mo is also discussed (30). In these works γ-alumina is mainly used as a support, and the performance of other aluminas is scarcely investigated (26).

In the present work we investigated the states of Mo supported on three kinds of aluminas (α-, γ-, and χ-aluminas) mainly by a XAFS technique combined with XRD, ESCA, and IR analyses. As α-alumina has scarcely and χ-alumina

[1] To whom correspondence should be addressed. E-mail: imamura@ipc.kit.ac.jp.

0021-9517/98 $25.00

has never been used as supports for Mo, it is of value to examine their performance. We have been interested in the liquid-phase epoxidation of olefins catalyzed by titanium (Ti) in titania-silica mixed oxide. This reaction is very sensitive to the configuration of the Ti; tetrahedral Ti is active due to the presence of coordinatively unsaturated site which can accommodate hydroperoxide (oxidizing reagent) in the first step of the reaction, while octahedral one is inactive (46, 47). As Mo is also a well-known epoxidation catalyst, it is interesting to investigate the effect of its configuration on its epoxidation activity. Thus, it is also the purpose of the present work to clarify the epoxidation activity of the supported Mo species on three kinds of aluminas in relation to their configuration. Allyl alcohol was used in the present epoxidation reaction. As Mo has much higher epoxidation activity than Ti and allyl alcohol is less reactive than other olefins such as oct-1-ene or cyclohexene, it is an appropriate reagent to differentiate the activities of the various Mo species present on the aluminas.

EXPERIMENTAL

Materials and Catalysts Preparation

t-Butyl hydroperoxide (TBHP) in benzene (50 wt%) and allyl alcohol were dried over molecular sieve 3 Å, and chlorobenzene over calcium chloride. Isopropanol was purified by 10 h of refluxing in the presence of calcium oxide, followed by distillation. Commercial K_2MoO_4 and $PbMoO_4$ were used for XAFS analysis as standard samples which have tetrahedral Mo and commercial MoO_3 and ammonium heptamolybdate(IV) $[(NH_4)_6Mo_7O_{24} \cdot 4H_2O]$ as standard octahedral Mo samples. MoO_4^{2-} with tetrahedral Mo and $Mo_7O_{24}^{6-}$ with octahedral Mo were obtained by adjusting the pH of the aqueous solution of $(NH_4)_6Mo_7O_{24} \cdot 4H_2O$ to 11 with ammonia and to 4.5 with 3 *N* nitric acid, respectively (12, 22, 44).

γ-Alumina and α-alumina were prepared by a sol–gel method. Aluminum(III) isopropoxide (204 g) in dry isopropanol (600 ml) was refluxed at 363 K for 2 h; 0.01 *N* aqueous acetic acid (360 ml) was added to the above solution, and the resultant alumina gel was allowed to age at 353 K for 5 days, followed by drying to give crystalline boehmite. γ-Alumina was obtained by calcining the boehmite at 1073 K in air for 5 h, and α-alumina at 1573 K in air for 3 h. χ-Alumina was synthesized according to the method developed by Inoue *et al.* (48). Aluminum(III) isopropoxide (13 g) was dissolved in 100 ml of p-xylene, and this solution was charged in an autoclave under a nitrogen atmosphere. The autoclave was maintained at 573 K for 3 h, and the resultant precipitate was washed with 20 ml of acetone and was dried. It was calcined at 873 K for 3 h in air, giving χ-alumina. The crystal phases of the three aluminas were identified by an XRD technique; χ-alumina was characterized by its peak at 2θ of 42.7° (d = 0.211 nm). BET surface areas of α-, γ-, and χ-aluminas were 6.0, 148.0, and 140.7 m^2/g, respectively.

Mo was loaded on the aluminas as follows. Alumina (3 g) was dispersed in deionized water containing a known amount of ammonium molybdate $[(NH_4)_6Mo_7O_{24} \cdot 4H_2O]$, and the mixture was stirred for 60 min. Then the solution was evaporated to dryness with an evaporator, followed by calcination of the solid portion at 773 K in air for 3 h.

Apparatus and Procedure

Chlorobenzene solution of allyl alcohol (0.2 *M*, 50 ml) and 1 ml of benzene containing 50 wt% of TBHP were charged in a 200-ml three-necked flask under a nitrogen atmosphere; the molar ratio of allyl alcohol to TBHP was 2. After TBHP was determined by an iodometry, a known amount of the catalyst (Mo, 1.04×10^{-4} mol) was added. Then the flask was immersed in an oil bath (363 K) to start the reaction under stirring with a magnetic agitator. The reaction was followed by monitoring the remaining TBHP, and 2,3-epoxypropan-1-ol was determined after the reaction was stopped (5 h).

Analysis

2,3-Epoxypropan-1-ol was determined with a Shimadzu GC-8A gas chromatograph with a PEG 20M column (3 m) at 393 K. It was also determined according to a hydrochloric acid–pyridine method on the basis of the amount of hydrochloric acid consumed by the epoxide (49).

The amount of the anionic hydroxyl groups on γ- and χ-aluminas was estimated by exchanging the OH groups with fluoride ion (50); γ-Alumina or χ-alumina (1.0 g) dried at 353 K overnight was dispersed in 25 ml of 0.057 *M* aqueous NH_4F for 3 days. After filtration, the remaining fluoride ion in the filtrate was determined with a Hitachi 075 potentiometer equipped with a fluoride electrode.

Molybdenum-supported alumina catalysts were sealed in a Q-pack pouch in a dry box for the X-ray absorption measurements. The absorption spectra were obtained at the beam line 6B station of the Photon Factory in the National Laboratory for High Energy Physics (Tsukuba) with a ring energy of 2.5 Gev and a ring current of 280–350 mA. A Si (311) double crystal was used to monochromatize the X rays. The spectra were recorded by a transmission mode at a room temperature in the range of the photon energies from 19.5 to 21.5 KeV for Mo K-edge (resolution energy of 4 eV at the edge). The method of the data analyses was described elsewhere (51, 52).

ESCA spectra were obtained with a Shimadzu ESCA 750 spectrophotometer, and the XRD data with a Rigaku Denki Geigerflex 2012 X-ray analyzer. IR analysis was carried out with a JEOL JIR-6500W FTIR spectrophotometer with a diffuse reflectance attachment and a Shimadzu

8200PC FTIR spectrophotometer. The catalysts were diluted to 5 wt% with KBr powder.

RESULTS AND DISCUSSION

ESCA, XRD, and IR Analyses

Figure 1 shows the effect of the amount of Mo-loading on the ESCA spectrum intensity ratio of Mo to Al. As the amount of Mo was increased, the ratio, I_{Mo}/I_{Al}, increased linearly to Mo-loading of about 15 and 18 wt% for χ- and γ-alumina, respectively; the linearity deviated upon further addition of Mo. The linear increase in I_{Mo}/I_{Al} with an increase in Mo implies that the Mo-monolayer is being formed in this Mo-loading region, and the deviation from the linearity indicates the formation of multilayers or aggregated Mo species (17, 43). The monolayer ended at a Mo-loading of only 1 wt% or less for α-alumina. As the surface areas of γ-alumina (148.0 m^2/g) and χ-alumina (140.7 m^2/g) were much larger than that of α-alumina (6.0 m^2/g), the difference in the behavior among the aluminas to form Mo-monolayer may be due only to the difference in their surface areas. However, when calcination temperature of Mo-loaded aluminas was increased from 773 to 923 K, $Al_2(MoO_4)_3$ was produced on γ- and χ-aluminas, while it was not formed on α-alumina irrespective of the amount of Mo loaded. Thus, surfaces of the former two are more active than that of the latter; as γ- and χ-aluminas are the transitional species in the course of transforming to the stable α-type, they should have higher reactivity. This situation is also shown in Fig. 2, in which the ESCA intensity ratio is plotted against the amount of Mo per unit surface area of the aluminas (mmol Mo/m^2). The patterns of Mo-monolayer formation are almost the same for all aluminas in the low Mo-loading region. However, the monolayer ended clearly at lower Mo-loading for α-alumina than for γ- and χ-aluminas, indicating the lower activity of the surface of the former. The result may also indicate that the surface of γ-alumina is more active than that of χ-alumina, although the monolayer end points for both are not so clear.

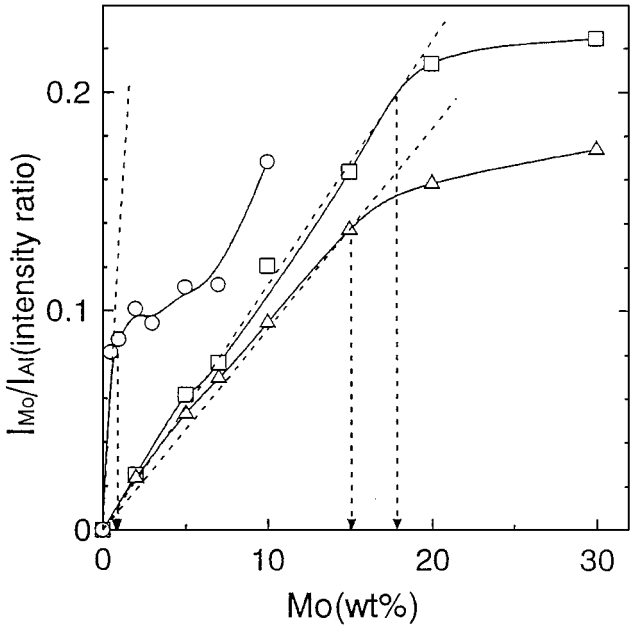

FIG. 1. ESCA analysis-I of Mo supported on (○) α-Al_2O_3, (□) γ-Al_2O_3, and (△) χ-Al_2O_3.

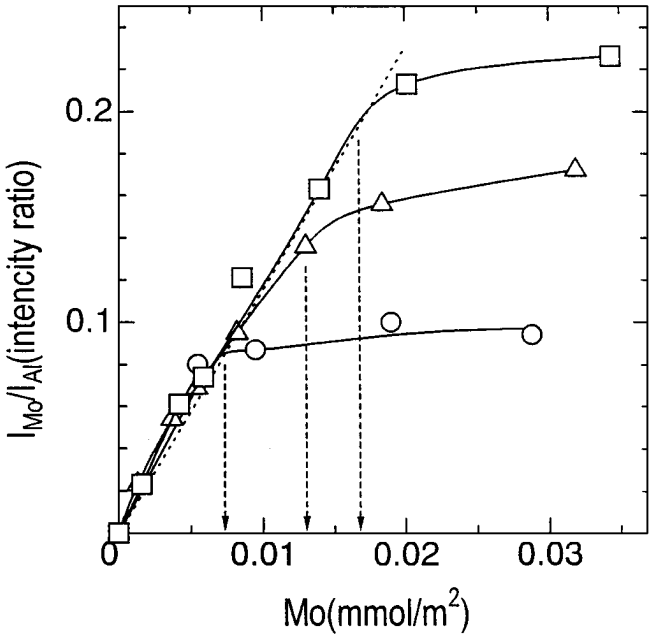

FIG. 2. ESCA analysis-II of Mo supported on (○) α-Al_2O_3, (□) γ-Al_2O_3, and (△) χ-Al_2O_3.

Figures 3 and 4 show the XRD patterns of Mo-supported γ- and α-aluminas. Peaks due to MoO_3 appeared at 2θ of 23 and 27° when 10 wt% of Mo was loaded on γ-alumina; no

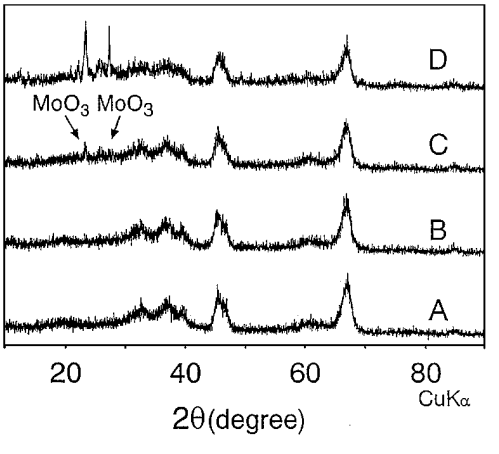

FIG. 3. XRD analysis of Mo supported on γ-Al_2O_3. Mo: (A) 5 wt%; (B) 7 wt%; (C) 10 wt%; and (D) 15 wt%.

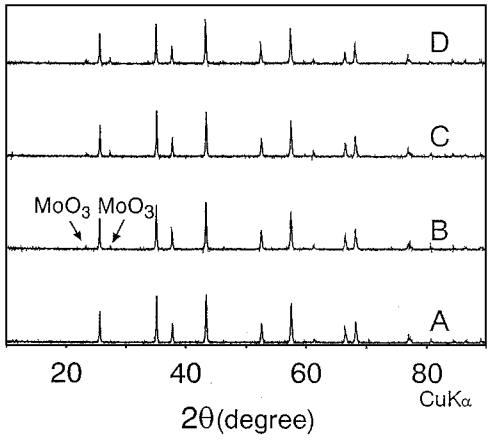

FIG. 4. XRD analysis of Mo supported on α-Al_2O_3. Mo: (A) 0.5 wt%; (B) 1 wt%; (C) 2 wt%; and (D) 3 wt%.

Mo diffraction peak was observed below 10 wt% loading (53). These peaks were also observed for χ-alumina supported with 10 wt% of Mo and above. On the other hand, MoO_3 was observed even with as low as 1 wt% of Mo-loading on α-alumina. Although ESCA data indicated that the monolayer was extended to 18 and 15 wt% of Mo loading on γ- and χ-alumina, respectively, the XRD analysis revealed that MoO_3 crystal phase was present in this monolayer region. Thus, the ESCA technique seems to overestimate the monolayer region. However, the linearity between I_{Mo}/I_{Al} and the amount of Mo-loading (ESCA result) gives us the image of the apparent monolayer development which accompanys the formation of a small amount of scattered MoO_3 islands detectable by the XRD analysis.

Figure 5 shows the IR spectra of Mo supported on γ-alumina measured by a transmission mode. The original spectra had been subtracted by the spectrum due to γ-alumina. Only one broad absorption band is observed at 914 cm^{-1} in the Mo=O vibrational stretching region for the samples with 3 and 5 wt% of Mo (12, 13). This band is not due to MoO_3 as shown below and is assumed to be due to surface-bound Mo species, probably octahedral (Oh) polymolybdate or isolated tetrahedral (Td) species. However, as there is no band of bridged Mo–O–Mo species in the lower wave number region, this band is ascribed to the isolated Td–Mo. The Mo=O stretching vibration becomes distinct at 953 cm^{-1} for 10 wt% Mo sample, and the band at 664 cm^{-1} due to Mo–O–Mo appears (13); polymolybdate is formed in addition to the isolated Td–Mo. At 15 wt% loading the bands of MoO_3 emerged at 599, 821, 873, and 995 cm^{-1}, which increased their intensity with the increase in Mo-loading. Although these bands were not observed in the 10 wt% sample, they may have been covered by the peaks due to polymolybdate and Td–Mo. The samples with 15 to 30 wt% of Mo have absorption band at 907 cm^{-1}. This band and the bands at 953 and 664 cm^{-1} are not observed for crystalline MoO_3; thus these are due to surface-bound Mo species. However, the band at 907 cm^{-1} could not be assigned, although it is surely due to some kind of Mo=O groups. The increase in the intensity of the 664 cm^{-1} band indicates the growth of polymolybdate species. The above IR analyses indicate the presence of a complicated mixture of Mo species on γ-alumina surface, especially for the samples with 15 to 30 wt% of Mo; Td–Mo, unidentified Mo, polymolybdate, and MoO_3 coexist. The IR spectra of Mo supported on χ-alumina exhibited the same pattern as those of Mo on γ-alumina without any difference to be mentioned specifically.

As a clear IR spectrum of the Mo on α-alumina could not be obtained by the transmission mode due to the strong absorption by α-Al_2O_3, diffuse reflectance spectra were obtained (Fig. 6). Although the band due to Mo=O of MoO_3 (995 cm^{-1}) appeared for the catalyst with 2 wt% of Mo and above, no other detailed information could be attained.

XAFS Analysis

We obtained further information on the states of the Mo species by a XAFS technique. Figure 7 shows the XANES

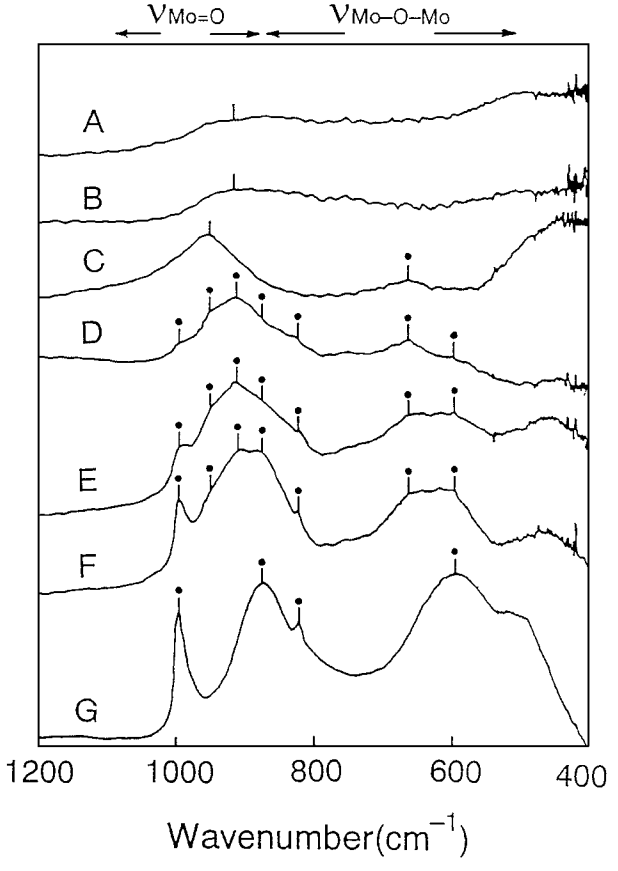

FIG. 5. IR spectra of Mo supported on γ-Al_2O_3. Mo: (A) 3 wt%; (B) 5 wt%; (C) 10 wt%; (D) 15 wt%; (E) 20 wt%; (F) 30 wt%; (G) MoO_3. All spectra were obtained by subtracting the spectrum of γ-Al_2O_3.

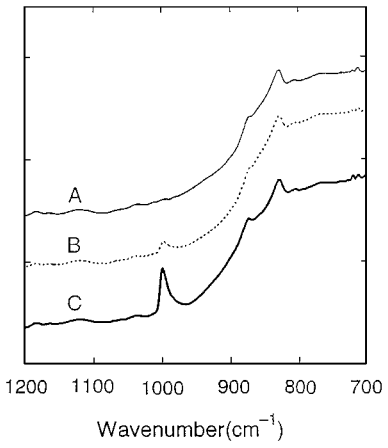

FIG. 6. IR spectra of Mo supported on α-Al_2O_3. Mo: (A) 0.5 wt%; (B) 2 wt%; (C) 7 wt%.

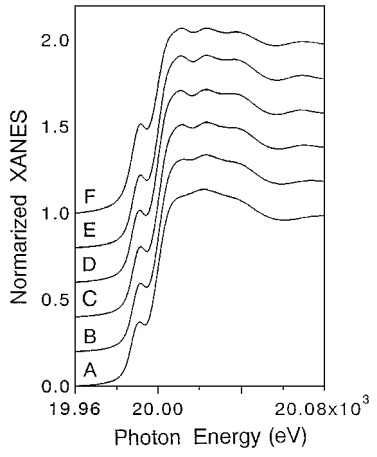

FIG. 8. XANES of Mo supported on α-Al_2O_3. Mo: (A) 0.5 wt%; (B) 1 wt%; (C) 2 wt%; (D) 7 wt%; (E) 15 wt%; (F) MoO_3.

spectra (Mo K-edge) of the standard samples. All samples show one pre-edge peak which is caused by the transition from 1s to 4d level of metal ions (26–28). Although this transition is formally forbidden, asymmetric configurations of metal ions allow it, and the intensity of the peak increases as the configuration of the metal ion deviates from octahedral symmetry (54). Thus the Td–Mo species [K_2MoO_4 (55), $PbMoO_4$ (27), and MoO_4^{2-} (25)] have larger pre-edge peaks than Oh–Mo's [MoO_3 (56), $Mo_7O_{24}^{6-}$ (57), and $(NH_4)_6Mo_7O_{24}$ (57)]. Other difference can be seen at the near-edge part of the spectra. Td–Mo's showed one relatively broad peak, while Oh species were characterized by a set of three small peaks. Thus the shapes of the pre-edge peak and of the near-edge region can be used to discriminate between Td– and Oh–Mo species.

The XANES spectra of the α-alumina samples are shown in Fig. 8. Although the pre-edge peaks did not differ so much with the difference in the amount of Mo loaded, a clear difference was observed for the near edge region. The sample with 0.5 wt% of Mo shows one broad peak suggesting the presence of Td species, whereas the one with 2 wt% of Mo shows three small peaks which resemble those of MoO_3. Further increase in Mo above 2 wt% did not result in any spectral change. The 1 wt% sample is characterized by a spectrum which is composed of the mixture of those for Td and Oh species. As shown in Fig. 9, according to the equation $[C = (A - f \times B)/(1 - f)$, f: $0 \le f < 1]$, the spectrum of 1 wt% sample (A) was subtracted by that of 0.5 wt% sample (B) with varying the value of f, followed by normalization. The optimization of this procedure gave the spectrum C

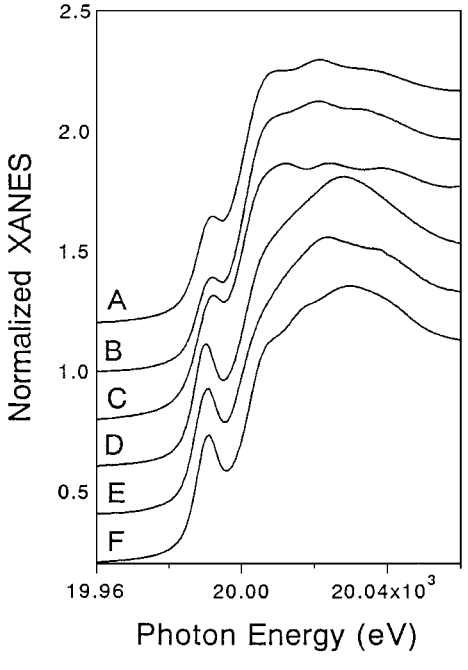

FIG. 7. XANES of standard samples. (A) $(NH_4)_6Mo_7O_{24}$, (B) $Mo_7O_{24}^{6-}$, (C) MoO_3, (D) K_2MoO_4, (E) $PbMoO_4$, (F) MoO_4^{2-}.

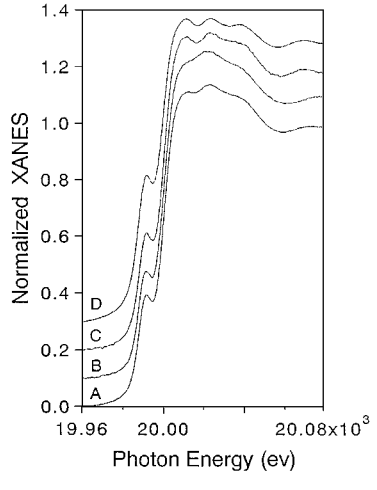

FIG. 9. XANES of Mo supported on α-Al_2O_3. (A) Mo 1 wt%, (B) Mo 0.5 wt%, (C) subtracted spectra A – B (see text), (D) MoO_3.

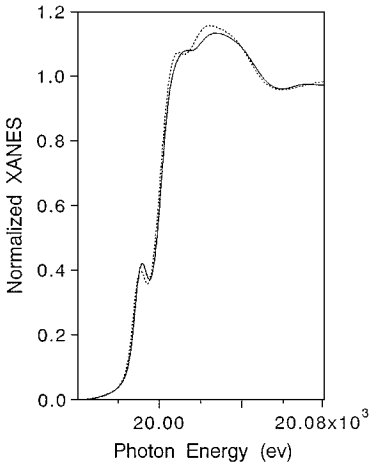

FIG. 10. XANES of Mo supported on γ-Al_2O_3. Mo: (·····) 1 wt%; (———) 30 wt%.

which exactly resembles that of MoO_3 (D), with the value of f, the fraction of B component (Td species) contained in A (mixture of Td and Oh), of 0.5. Thus, 50% of the Mo in 1 wt% sample is composed of the Td species. This is in accord with the ESCA result that the monolayer formation completed at a Mo-loading of 1 wt% or less, and MoO_3 was actually detected at 1 wt% of Mo-loading by an XRD technique.

The XANES spectra of Mo on γ- and χ-aluminas were very similar and did not show a clear change with the amount of Mo-loading; shown in Fig. 10 are the spectra of 1 and 30 wt% samples (γ-alumina). Although MoO_3 should surely be formed for 30 wt% sample, its XANES spectrum does not have the three peaks characteristic of MoO_3. Although the slight difference in the two XANES spectra may indicate a change from Td to Oh characteristic, details are not known now.

The Fourier transforms (FT) of the EXAFS spectra of the standard samples are shown in Fig. 11. The FT's of the Td–Mo samples (D ~ F) have a single peak due to four equivalent Mo–O bonds. The Oh–Mo in MoO_3 has two peaks due to Mo=O and Mo–O bonds in the first shell region although the latter peak is not so distinct for other Oh–Mo samples. The peak at longer distance (about 3 Å) for Oh–Mo species is ascribed to Mo–Mo interaction; the reason for the absence of the corresponding peak for Td-samples is not known. Shown in Fig. 12 are the FT's of the EXAFS oscillation for the Mo on α-alumina. As the phase shift correction was not applied, the apparent bond distance is shorter than the real one. A distinct change is observed in the Mo-loading between 0.5 and 2%. The 0.5 wt% sample shows only one peak at a distance of 1.2 Å. The curve-fitting for the back Fourier transform of this peak (between 0.7 and 1.8 Å) gave the Mo–O bond distance of 1.77 Å; this bond distance is shorter than that of the Oh–Mo's such as MoO_3 and $Mo_7O_{24}^{6-}$ (26). Thus combined with the XANES result, this Mo species was identified as Td–Mo. The samples with 2 wt% of Mo and above have two kinds of Mo–O bonds (0.7–2.0 Å) and a Mo–Mo interaction (2.7–4.0 Å), which are very much like with those of MoO_3; thus, MoO_3 is formed. The FT of 1 wt% sample has an intermediate characteristic between 0.5 wt% sample and 2 wt% sample, which is also in good agreement with the result of XANES analysis that Td–Mo and MoO_3 coexist. The FT's for γ-alumina samples are shown in Fig. 13. The samples containing 1 and 2 wt% of Mo show only one Mo–O peak, which is due to the isolated Td–Mo. However, adjacent Mo–Mo interaction begins to appear for 5 wt% sample and above, indicating the aggregation of the Td species. As the IR analyses indicated the presence of polymolybdate in the 10 wt% sample, two peaks observed for the 10 wt% sample seem to include the Mo–O and Mo–Mo interactions of the polymolybdate in addition to those of the Td–Mo. However, the presence of MoO_3 as evidenced by the XRD analysis was not confirmed from the spectrum of the 10 wt% sample. For 15 wt% sample the

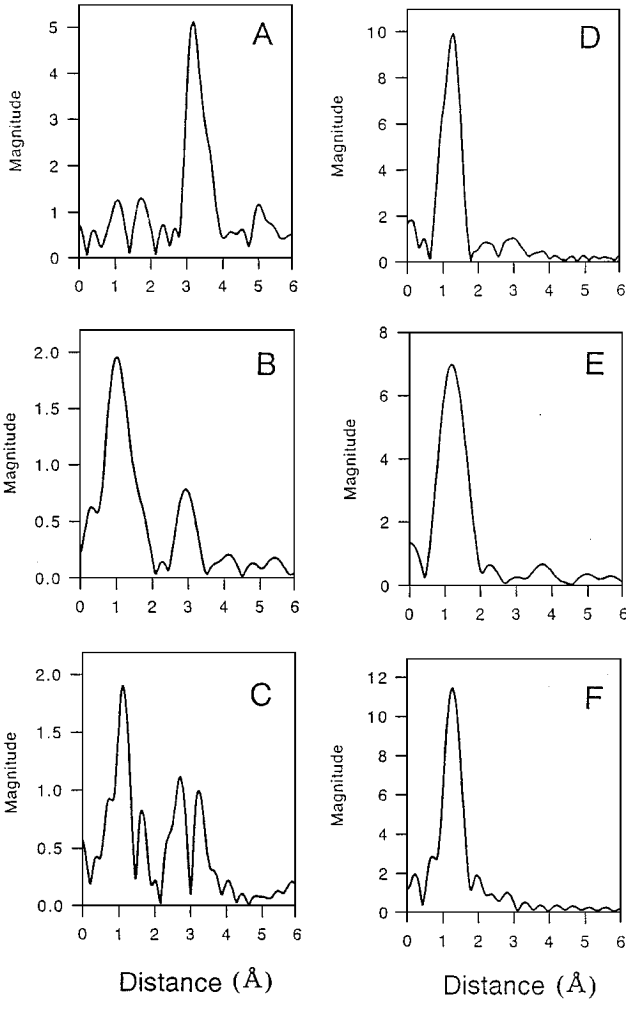

FIG. 11. EXAFS-FT of standard samples. (A) MoO_3, (B) $Mo_7O_{24}^{6-}$, (C) $(NH_4)_6Mo_7O_{24}$, (D) K_2MoO_4, (E) $PbMoO_4$, (F) MoO_4^{2-}.

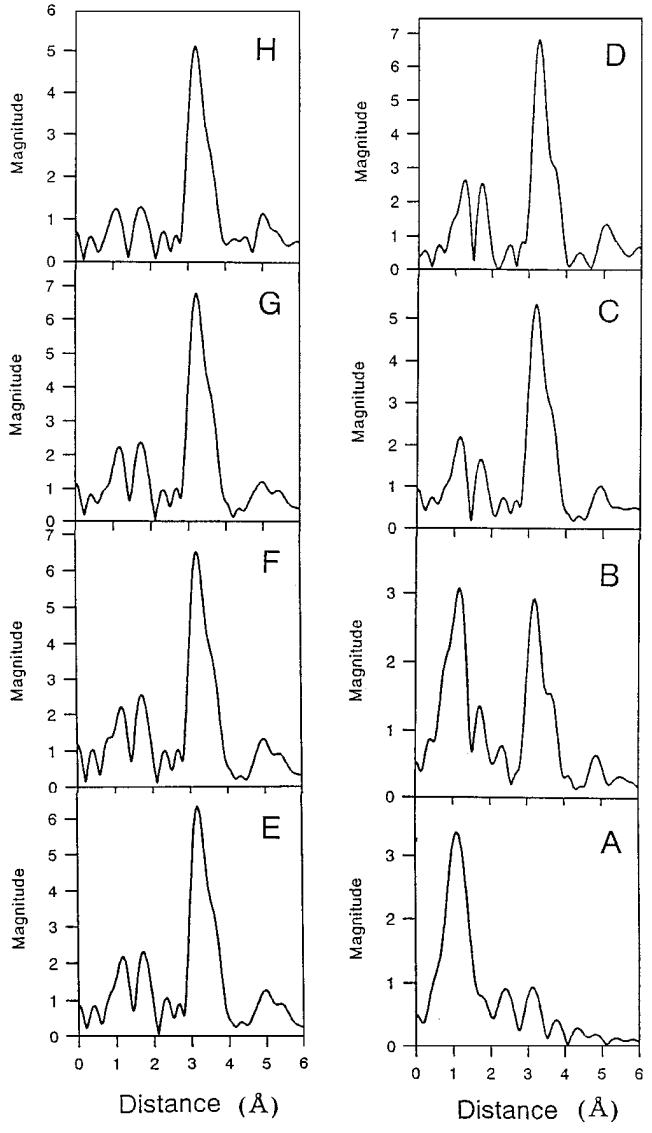

FIG. 12. EXAFS-FT of Mo supported on α-Al_2O_3. Mo: (A) 0.5 wt%; (B) 1 wt%; (C) 2 wt%; (D) 3 wt%; (E) 5 wt%; (F) 7 wt%; (G) 10 wt%; (H) MoO_3.

Mo–O peak due to Oh–Mo of MoO_3 begins to appear, and this peak intensity increases with an increase in Mo-loading, together with the increment in the Mo–Mo peak intensity. The intensity of the peak of Mo–O due to Td–Mo (and polymolybdate) is still large for the sample with as much as 30 wt% of Mo, suggesting that Td–Mo (and polymolybdate) and MoO_3 coexist with comparable amounts even at this high Mo-loading region. This situation is very much the same as that observed in the IR experiment (Fig. 5). The mode of the formation of Mo species on χ-alumina is almost the same as that on γ-alumina with a slight difference in the effect of the amount of Mo-loading (Fig. 14). For example the region of the formation of isolated Td species as deduced from the absence of the peak near 3 Å (Mo–Mo) is seems to be extended to 5 wt% loading, although the BET surface area is a little larger for γ-alumina (148.0 m^2/g) than for χ-alumina (140.7 m^2/g). As isolated Mo species is formed preferentially by an exchange with the anionic hydroxyl group on alumina (10, 34, 58), its amount may be larger on χ-alumina. To check this possibility, the surface hydroxyl group was determined by an exchange with fluoride ion. The amount was 3.39×10^{-6} mol/m^2 on γ-alumina and 3.20×10^{-6} mol/m^2 on χ-alumina; there is almost no difference between the two. Thus the reason for the abundance of the isolated Td–Mo on χ-alumina is not known.

Epoxidation of Allyl Alcohol

The results of the epoxidation of allyl alcohol are summarized in Table 1, and Fig. 15 shows the selectivity

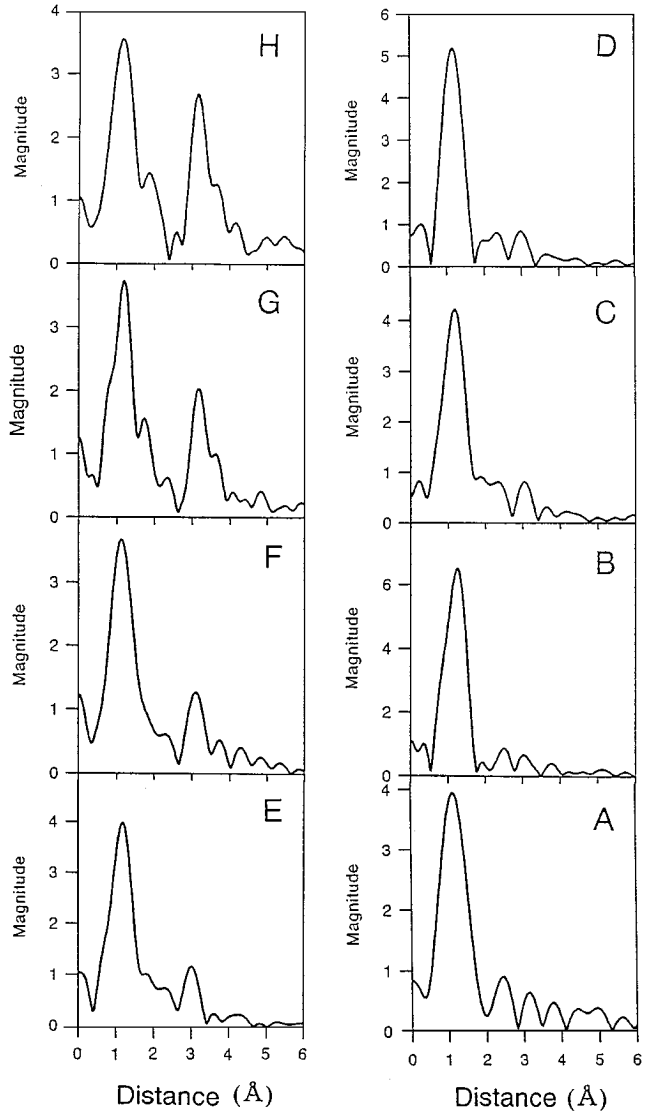

FIG. 13. EXAFS-FT of Mo supported on γ-Al_2O_3. Mo: (A) 1 wt%; (B) 2 wt% (C) 5 wt%; (D) 7 wt%; (E) 10 wt%; (F) 15 wt%; (G) 20 wt%; (H) 30 wt%.

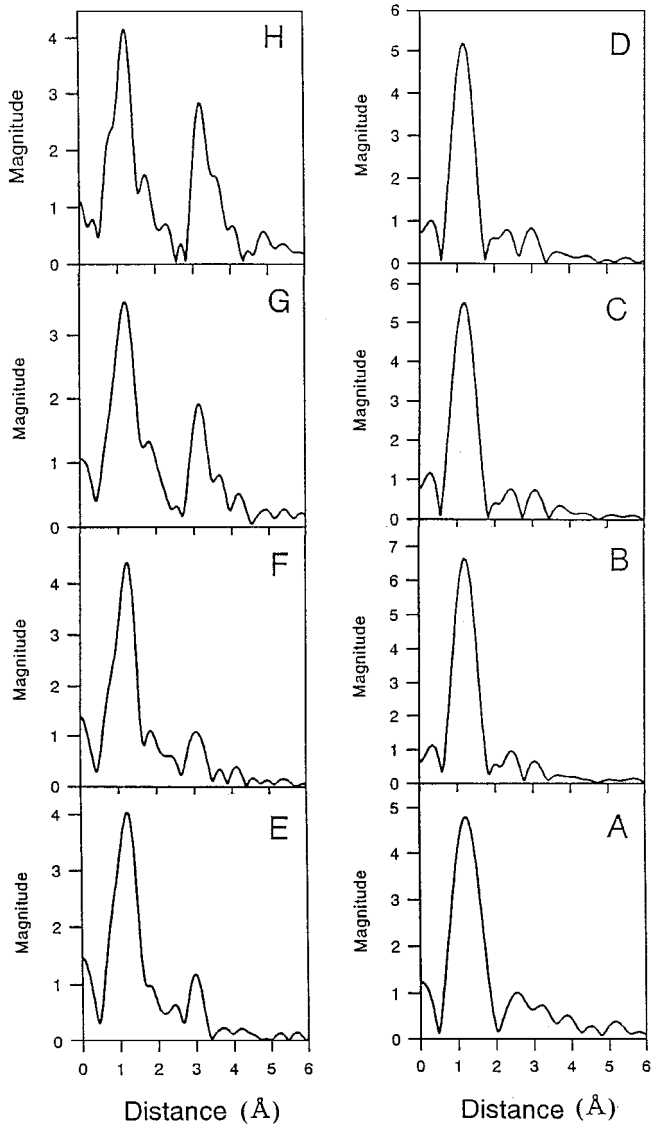

FIG. 14. EXAFS-FT of Mo supported on χ-Al_2O_3. Mo: (A) 1 wt%; (B) 2 wt%; (C) 5 wt%; (D) 7 wt%; (E) 10 wt%; (F) 15 wt%; (G) 20 wt%; (H) 30 wt%.

of 2,3-epoxypropan-1-ol as a function of the amount of Mo loaded. The yield and, especially, the selectivity of 2,3-epoxypropan-1-ol increased with an increase in the Mo-loading. The selectivity increase is milder for γ- and χ-aluminas than for α-alumina; nearly 90% or higher selectivity was obtained on the latter with a Mo-loading of 2 wt% and above. The comparison of the result shown in Fig. 15 with the ESCA results (Fig. 1) indicates that the monolayer Mo species on all aluminas are not so effective for the epoxidation. Especially the isolated Td–Mo species at low Mo loading (2 wt% for γ-alumina and 5 wt% for χ-alumina) (XAFS result: Figs. 13 and 14) were completely inactive.

The Oh–Mo species are more active for the epoxidation than Td species; especially isolated Td–Mo is completely inactive as shown above. MoO_3 seems to have the highest selectivity. In a separate experiment, a 100% of the selectivity to 2,3-epoxypropan-1-ol was obtained under the same reaction condition using MoO_3 powder (Mo, 1.04×10^{-4} mol), although the conversion of TBHP was only 6.7%. This result is quite unexpected because previous work shows that Td species of titanium, zirconium, and niobium incorporated in a silica matrix are active for the epoxidation of oct-1-ene or cyclohexene, while Oh species are inactive (46, 47, 59, 60). As the normal configuration of these metal ions is Oh, we deduced that epoxidation is initiated by the coordination of a hydroperoxide (oxidant) to the unsaturated site of these metal ions only when they are in the Td environment. However, the present result compelled us to consider another reaction mechanism for the epoxidation of allyl alcohol catalyzed by Mo. There is abundant evidence that MoO_3 interacts with hydroperoxides, giving monoperoxo-type or diperoxo-type Mo species, and these peroxo-type Mo effectively epoxidize olefins (61–64). Thus the peroxo-type Mo may be an active intermediate in the present reaction. To check this possibility, epoxidation was carried out over Mo supported on γ-alumina with 5 and 30 wt% loading. After the reaction for 1 h the catalyst was filtered, washed with n-hexane, and was subjected to air-drying at a room temperature. The active oxygen on the catalysts as determined iodometrically was 8.0×10^{-6} and

TABLE 1

Epoxidation of Allyl Alcohol[a]

Support	Mo (%)	TBHP decompd. (%)	Epoxide select (%)	Epoxide yield (%)
γ-Al_2O_3	2	10	0	0
	5	36.8	37.7	13.8
	7	56.1	41.1	23.1
	10	68.7	45.4	31.2
	15	66.1	70.8	46.8
	20	65.6	69.0	45.3
	30	60.0	94.2	56.5
χ-Al_2O_3	2	12.8	0	0
	5	18.9	0	0
	7	36.5	41.3	15.1
	10	66.9	51.4	34.4
	15	74.2	59.3	44.0
	20	77.9	76.3	59.4
	30	76.6	83.2	63.7
α-Al_2O_3	0.5	74.3	54.4	40.4
	1	76.8	59.8	45.9
	2	80.6	89.5	72.1
	3	73.7	85.9	63.0
	5	65.0	91.5	59.4
	7	59.9	86.6	51.9
	10	51.4	99.8	51.2
	15	79.4	97.5	77.4

[a] Temperature, 363 K; reaction time, 5 h. Other reaction conditions are shown in the experimental section.

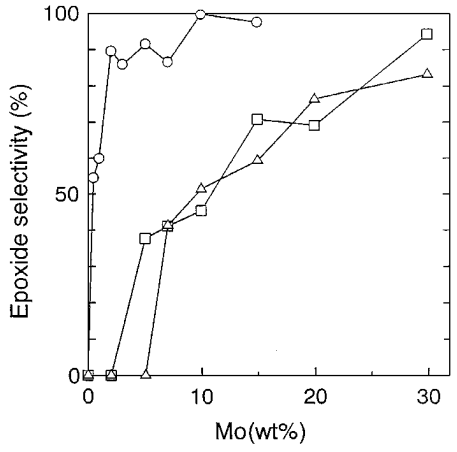

FIG. 15. Epoxidation of allyl alcohol over Mo supported on (○) α-Al_2O_3, (□) γ-Al_2O_3, and (△) χ-Al_2O_3. Temperature, 363 K; reaction time, 5 h. Other reaction conditions are shown in the experimental section.

6.0×10^{-5} mol/g for 5 and 30 wt% samples, respectively; the same treatment having been done for γ-alumina alone as a blank test to eliminate the contribution from the absorbed TBHP on it. Therefore, the route of the epoxidation may involve the formation of peroxo-type Mo species by an interaction of TBHP with the Oh–Mo's including MoO_3 on the alumina. Although we tried to obtain the evidence for the presence of peroxo-type oxygen by an IR technique (540 and 590 cm^{-1}), the strong absorption band of γ-alumina prevented its detection (65). The reason why Td–Mo is inactive or has, if any, only a low activity is not known, and further investigation is needed to clarify the details.

If the peroxo-type Mo is formed during the reaction via the restructure of the supported Mo, it may indicate that the Mo on alumina is unstable and the homogeneous Mo eluted into the solution works as a main catalyst. Actually, the supported Mo was not robust. However, the homogeneous Mo, which was eluted from the catalyst, had only a very low epoxidation activity. The Mo supported on γ-alumina (30 wt%) was kept in the reaction mixture without allyl alcohol at 363 K for 2 h. After the solution was filtered, allyl alcohol and an additional amount of TBHP were added to the filtrate and the epoxidation was carried out for 5 h. A 36.3% of TBHP was decomposed and the epoxidation selectivity was 19.6%. When Mo supported on γ-alumina (30 wt%) was used, 60.0% of TBHP was decomposed and the epoxidation selectivity was 94.2%. This difference, especially the difference in the selectivity, indicates that the active species in the epoxidation is not the eluted Mo but the Mo supported on aluminas. Therefore, the discussion given here concerning the relationship between the epoxidation activity and the state of the supported Mo is validly done despite the liability that the elution of a part of Mo does occur.

ACKNOWLEDGMENTS

This work was performed under the approval of the Photon Factory Advisory Committee of National Institute of High Energy Physics (Proposal No. 94G006). The authors are indebted to Professor Nomura and Mr. Koyama of KEK-PF of Tsukuba for the XAFS experiment. They also express their gratitude to Dr. T. Tanaka of Kyoto University for his permission to use his XANES analysis program. The simulation was carried out with a FACOM M780/30 computer at the Data Processing Center of Kyoto University. Thanks are also due to Dr. T. Ito of Otsuma Women's University and Dr. E. Yamada and Mr. K. Utani of Kyoto Institute of Technology for their kind cooperation.

REFERENCES

1. Okamoto, Y., Tomioka, H., Katoh, Y., Imanaka, T., and Teranishi, S., *J. Phys. Chem*. **84**, 1833 (1980).
2. Okamoto, Y., Imanaka, T., and Teranishi, S., *J. Phys. Chem*. **85**, 3798 (1981).
3. Ono, T., Anpo, M., and Kubokawa, Y., *J. Phys. Chem*. **90**, 4780 (1986).
4. Niwa, M., Yamada, H., and Murakami, Y., *J. Catal*. **134**, 331 (1992).
5. Matuoka, Y., Niwa, M., and Murakami, Y., *J. Phys. Chem*. **94**, 1477 (1990).
6. Miyata, H., Tokuda, S., Ono, T., Ohno, T., and Hatayama, F., *J. Chem. Soc., Faraday Trans*. **86**, 2291 (1990).
7. Ono, T., Nakagawa, Y., Miyata, H., and Kubokawa, Y., *Bull. Chem. Soc. Jpn* **57**, 1205 (1984).
8. Miyata, H., Tokuda, S., Ono, T., Ohno, T., and Hatayama, F., *J. Chem. Soc., Faraday Trans*. **86**, 3659 (1990).
9. Quincy, R. B., Houalla, M., Proctor, A., and Hercules, D. M., *J. Phys. Chem*. **94**, 1520 (1990).
10. Jeziorowski, H., and Knözinger, H., *J. Phys. Chem*. **83**, 1166 (1979).
11. Ono, T., Miyata, H., and Kubokawa, Y., *J. Chem. Soc., Faraday Trans. 1* **83**, 1761 (1987).
12. Giordano, N., Bart, J. C. J., Vaghi, A., Castellan, A., and Martinotti, G., *J. Catal*. **36**, 81 (1975).
13. Mortimer, R., Powell, J. G., Greenblatt, M., McCarroll, W. H., and Ramanujachary, K. V., *J. Chem. Soc., Faraday Trans*. **89**, 3603 (1993).
14. Louis, C., Che, M., and Anpo, M., *J. Catal*. **141**, 453 (1993).
15. Rodrigo, L., Marcinkowska, K., Adnot, A., Roberge, P. C., Kaliaguine, S., Stencel, J. M., Makovsky, L. E., and Diehl, J. R., *J. Phys. Chem*. **90**, 2690 (1986).
16. Zingg, D. S., Makovsky, L. E., Tischer, R. E., Brown, F. R., and Hercules, D. M., *J. Phys. Chem*. **84**, 2898 (1980).
17. Sarrazin, P., Kasztelan, S., Payen, E., Bonnelle, J. P., and Grimblot, J., *J. Phys. Chem*. **97**, 5954 (1993).
18. Dufresne, P., Payen, E., Grimblot, J., and Bonnelle, J. P., *J. Phys. Chem*. **85**, 2344 (1981).
19. Grünert, W., Stakheev, A. U., Mörke, W., Feldhaus, R., Anders, K., Shpiro, E. S., and Minachev, K. M., *J. Catal*. **135**, 269 (1992).
20. Bianchi, C. L., Gattania, M. G., and Villa, P., *Appl. Sur. Sci*. **70/71**, 211 (1993).
21. Spevack, P. A., and McIntyre, N. S., *J. Phys. Chem*. **97**, 11020 (1993).
22. Wang, L., and Hall, W. K., *J. Catal*. **66**, 251 (1980).
23. Desikan, A. N., Huang, L., and Oyama, S. T., *J. Chem. Soc. Faraday Trans*. **88**, 3357 (1992).
24. Mitchell, P. C. H., Tomkinson, J., Grimblot, J. G., and Payen, E., *J. Chem. Soc., Faraday Trans*. **89**, 1805 (1993).
25. Chiu, N. S., Bauer, S. H., and Johnson, M. F. L., *J. Catal*. **89**, 226 (1984).
26. Clausen, B. S., Topsøe, H., Candia, R., Villadsen, J., Lengeler, B., Als-Nielsen, J., and Christensen, F., *J. Phys. Chem*. **85**, 3868 (1981).
27. Bare, S. R., Mitchell, G. E., Maj, J. J., Vrieland, G. E., and Gland, J. L., *J. Phys. Chem*. **97**, 6048 (1993).
28. Cramer, S. P., Hodgson, K. O., Gillum, W. O., and Mortenson, L. E., *J. Am. Chem. Soc*. **100**, 3398 (1978).

29. Verbruggen, N. F. D., Mestl, G., Von Hippel, L. M. J., Lengeler, B., and Knözinger, H., *Langmuir* **10**, 3063 (1994).
30. Mensch, C. T. J., Van Veen, J. A. R., Van Wingerden, B., and Van Dijk, M. P., *J. Phys. Chem*. **92**, 4961 (1988).
31. Hedman, B., Frank, P., Gheller, S. F., Roe, A. L., Newton, W. E., and Hodgson, K. O., *J. Am. Chem. Soc.* **110**, 3798 (1988).
32. Sarrazin, P., Mouchel, B., and Kasztelan, S., *J. Phys. Chem*. **93**, 904 (1989).
33. Sarrazin, P., Mouchel, B., and Kasztelan, S., *J. Phys. Chem*. **95**, 7405 (1991).
34. Diaz, A. L., and Bussell, M. E., *J. Phys. Chem*. **97**, 470 (1993).
35. Liu, H. C., and Weller, S. W., *J. Catal.* **66**, 65 (1980).
36. Weller, S. W., *Acc. Chem. Res.* **16**, 101 (1983).
37. Tauster, S. J., Pecoraro, T. A., and Chianelli, R. R., *J. Catal.* **63**, 515 (1980).
38. Millman, W. S., Bartholomew, C. H., and Richardson, R. L., *J. Catal.* **90**, 10 (1984).
39. Nag, N. K., *J. Catal.* **92**, 432 (1985).
40. Segawa, K., and Hall, W. K., *J. Catal.* **77**, 221 (1982).
41. Gil-Llambias, F. J., Escudey-Castro, A. M., Agudo, A. L., and Carcia-Fierro, J. L., *J. Catal.* **90**, 323 (1984).
42. Niwa, M., Inagaki, S., and Murakami, Y., *J. Phys. Chem*. **89**, 3869 (1985).
43. Spanos, N., and Lycourghiotis, A., *J. Catal.* **147**, 57 (1994).
44. Acro, M. D., Garrazán, S. R. G., Rives, V., and Garcia-Ramos, J. V., *J. Mater. Sci.* **27**, 5921 (1992).
45. Medema, J., Van Stam, C., De Beer, V. H. J., Konings, A. J. A., and Koningsberger, D. C., *J. Catal.* **53**, 386 (1978).
46. Imamura, S., Nakai, T., Kanai, H., and Ito, T., *Catal. Lett.* **28**, 277 (1994).
47. Imamura, S., Nakai, T., Kanai, H., and Ito, T., *J. Chem. Soc., Faraday Trans.* **91**, 1261 (1995).
48. Inoue, M., Kominami, H., and Inui, T., *J. Am. Ceram. Soc.* **75**, 2597 (1992).
49. Kimura, K. (Ed.), "Bunseki Kagaku Benran," p. 334, Maruzen, Tokyo, 1981.
50. Yamagata, N., Owada, Y., Okazaki, S., and Tanabe, K., *J. Catal.* **47**, 358 (1977).
51. Yoshida, S., Tanaka, T., Hanada, T., Hiraiwa, T., Kanai, H., and Funabiki, T., *Catal. Lett.* **12**, 277 (1992).
52. Kanai, H., Mizutani, H., Tanaka, T., Funabiki, T., Yoshida, S., and Takano, M., *J. Mater. Chem*. **2**, 703 (1993).
53. Smith, J. V. (Ed.), "X-Ray Powder Data File," Sets 1–5, p. 629, Amer. Soc. for Testing and Materials, Philadelphia, 1967.
54. Kutzler, F. W., Natoli, C. R., Misemer, D. K., Doniach, S., and Hodgson, K. O., *J. Chem. Phys.* **73**, 3274 (1980).
55. Gatehouse, B. M., and Leverett, P., *J. Chem. Soc. Ser. A*, 849 (1969).
56. Kihlborg, L., *Ark. Kem.* **21**, 357 (1963).
57. Evans, H. T., Jr., *J. Am. Chem. Soc.* **90**, 3275 (1968).
58. Okamoto, Y., and Imanaka, T., *J. Phys. Chem*. **92**, 7102 (1988).
59. Kawabata, S., Imamura, S., and Kanai, H., *in* "Proceeding of the Annual Meeting of the Catalysis Society of Japan (A), Fukuoka, October, 1996," p. 158.
60. Yamashita, T., Imamura, S., and Kanai, H., *in* "Proceeding of the Annual Meeting of the Catalysis Society of Japan (A), Fukuoka, October, 1996," p. 159.
61. Mimoun, H., Seree De Roch, I., and Sajus, L., *Tetrahedron* **26**, 37 (1979).
62. Jörgensen, K. A., *Chem. Rev.* **89**, 431 (1989).
63. Arakawa, H., Moro-oka, Y., and Ozaki, A., *Bull. Chem. Soc. Jpn.* **47**, 2958 (1974).
64. Arakawa, H., and Ozaki, A., *Chem. Lett.*, 1245 (1975).
65. Ishii, Y., and Ogawa, M., "Reviews on Heteroatom Chemistry," Vol. 3 (S. Oae, Ed.), p. 121, MYU, Tokyo, 1990.